High-precision equation of state benchmark for cryogenic liquid deuterium at ultrahigh pressure

Zhiyu He [1,*] Qili Zhang,[2,*] Haifeng Liu [2,†] Guo Jia [1,‡] Xiuguang Huang,[1] Zhiheng Fang,[1] Zhiyong Xie,[1] Junjian Ye,[1]
Hua Shu,[1] Jiaqin Dong,[1] Fan Zhang,[1] Yuchun Tu,[1] Wei Wang,[1] and Sizu Fu[1]

[1]*Shanghai Institute of Laser Plasma, P. O. BOX 800229, Shanghai 201800, China*
[2]*Laboratory of Computational Physics, Institute of Applied Physics and Computational Mathematics, Beijing 100094, China*

We provide a principal Hugoniot of cryogenic liquid deuterium at a pressure of $27 < P < 240$ GPa, with reflected-shock data of up to ∼830 GPa. The maximum density reaches ∼1.49 g/cm^3, about 8.7 times the initial density. Our independent principal Hugoniot experimental data broadly support the wide-regime equation of state (WEOS) model, which well matches Fernandez-Pañella *et al.* [Phys. Rev. Lett. **122**, 255702 (2019)] and Knudson *et al.* [Phys. Rev. Lett. **118**, 035501 (2017)] experimental data over the observed pressure range up to 550 GPa, and most of three sets of reflected shock data are in accordance with our theory up to 1 TPa. Our high-precision experimental results establish an important benchmark equation of state of deuterium and conform to the WEOS model quite well. Our work is useful for the development of the high-pressure response of hydrogen's isotopes, directly related to inertial confinement fusion, planetary science, and metallization.

I. INTRODUCTION

Hydrogen, the most abundant and simple element, has a considerably complex phase diagram at high pressure and so is important in modern condensed-matter theory and numerical simulation [1]. A major component of many celestial bodies [2], hydrogen's properties at high pressure, density, and temperature are key in stellar structure and the formation and evolution of gas planets [3,4]. Moreover, hydrogen and its isotopes are important in inertial confinement fusion (ICF) [5]. The equation of state (EOS) of hydrogen under the strongest first shock in ICF continues to predominate high energy density physics [6–9]. The behavior of hydrogen near its metal-insulator transition has garnered much scientific interest [10]. Dense hydrogen dissociates into conductive fluid under extreme high pressure [11–13]. Therefore, it is necessary to accurately test the EOS of hydrogen and its isotopes and extend the benchmark database to include higher pressures.

Dynamic compression experiments are mainly used to study the properties of hydrogen and deuterium at high pressure. Specifically, the Hugoniot curve and the density compressibility of deuterium are key for theoretical models under extreme conditions. Compression as a function of pressure in theoretical models varies greatly [14,15]. Therefore, scientists have been developing reliable experimental methods to meet the needs of theoretical modeling. Nellis *et al.* [16] measured the single-shock D_2 at low pressure using a gas gun (∼21 GPa). Spherical convergence compression experiments by Boriskov *et al.* [17,18] and Grishechkin *et al.* [19]

reached ∼121 GPa, and the maximum compression reached ∼4.5 around 100 GPa. Knudson *et al.* [20,21] achieved high-precision Hugoniot results at 21–176 GPa on a Z machine, revealing that the maximum compression was at relatively low pressure (∼50 GPa). However, the pressure of the Z machine platform is limited to ∼200 GPa with the plane shocks used so far. Regarding laser devices, the maximum compression obtained by Da Silva *et al.* [5] reached ∼6, different from other experimental results. Subsequently, Hicks *et al.* [22] obtained Hugoniot data for liquid deuterium at 45–220 GPa, indicating that the compression was less than 4.2 below 100 GPa, reaching a maximum value of ∼5 between 100 and 220 GPa. Recently, the results worthy of attention published by Fernandez-Pañella *et al.* [23] reported the high-precision principal Hugoniot data of D_2 up to 550 GPa and reflected shock data up to ∼1 TPa. Their low-pressure (<200 GPa) results were consistent with those of a Z machine [21], and these two works can distinguish reliably among the various theoretical models in the molecular-to-atomic (MA) transition region (50–120 GPa).

However, no single model consistently described all the details in the principal Hugoniot of liquid D_2 in the pressure range of 40 to 550 GPa until recently. Another fact is that Fernandez-Pañella *et al.* [23] only gave the reshock data of four points and lacked low-pressure data below 200 GPa. Also, their reshock compression of deuterium above 500 GPa is 5%–7% higher than the current theoretical models. Therefore, abundant high-precision reshock experimental data in a wider pressure range are needed to provide evidence for theory models.

In view of the above two questions, this work reports the principal Hugoniot data of cryogenic liquid deuterium at a pressure of $27 < P < 240$ GPa and its reflected-shock data of up to ∼830 GPa. The maximum density of D_2 reaches ∼1.49 g/cm^3, about 8.7 times the initial density. Our independent

*These authors contributed equally to this work.

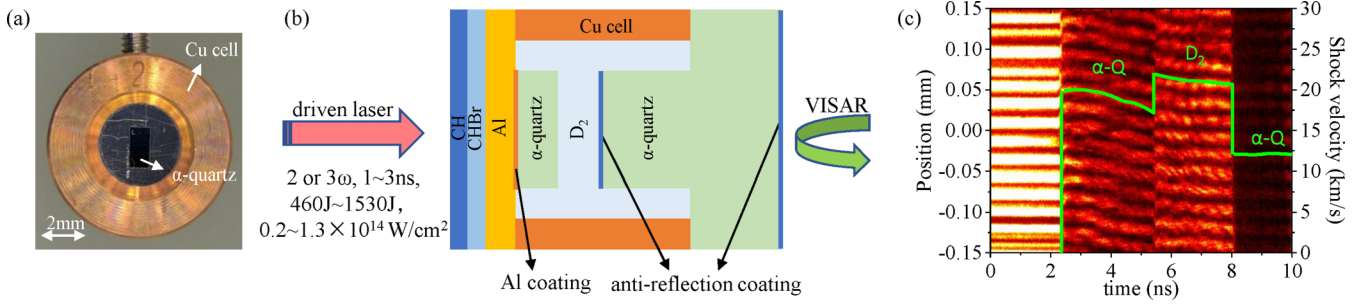†liu_haifeng@iapcm.ac.cn

‡387890448@qq.com

FIG. 1. (a) Real picture of the cryogenic deuterium target. (b) Schematic of the cryogenic deuterium target. (c) Raw VISAR image for shot 15035, showing continuous tracking of the shock front within both D_2 and α-quartz. The corresponding velocity profile (green curve) is also shown.

principal and reflected experimental data well conform to our wide-regime equation of state (WEOS) model within a wide pressure range (27–830 GPa), which is important for the verification of the deuterium EOS model and the construction of a benchmark database.

II. DETAILS OF EXPERIMENT AND MODEL

A. Experiment

Experiments were carried out using the Shenguang-II Nd:glass laser of the National Laboratory of High Power Laser and Physics. The ninth laser of Shenguang-II was vertically incident to the target to maximize the target's absorption efficiency from the laser. Shock waves were generated by ablation of a thin plastic layer backing the sample. Energies of 460–1530 J were delivered in a 1–3-ns pulse at 351 or 527 nm. The laser beam was smoothed using a lens-array (LA) system [24,25] to eliminate large-scale spatial modulation and to obtain a flat-topped profile in the focal plane. The characteristics of the optical system (lens + LA) were such that the focal spot was a 1×0.7 or 0.5×0.7 mm^2 rectangular flat region. The resulting intensities were 0.2–1.3 $\times$ 10^{14} W/cm^2.

The real picture and the experimental design of the target are shown in Figs. 1(a) and 1(b), respectively. The cryogenic liquid deuterium was contained in a copper cell and sandwiched between a standard material and a stepped cylindrical α-quartz window ($\sim$700-μm thick). The standard material used for impedance matching [14,26,27] was 50–60-μm α-quartz [28–31] with an aluminum coating (20-μm aluminum steps were used in several shots) and adhered on an $\sim$35-μm thick polished aluminum buffer. The buffer was coated on the reverse side with $\sim$25-μm polyimide doped with bromine (CHBr) and an $\sim$15-μm polyimide (CH) ablation layer. The stepped cylindrical α-quartz window was situated 50–60 μm away from the standard material and was coated on both sides with an antireflection coating centered at 540 or 660 nm for the velocity interferometer system for any reflector (VISAR) [32,33] probe beam to minimize ghost reflections. The experiment was carried out at $\sim$20.5 K using a cryogenic platform. The initial density ρ_0 of the cryogenic liquid deuterium was 0.170 ± 0.001 g/cm^3, calculated by the empirical formula [13,34,35], and the initial density of α-quartz was 2.65 g/cm^3.

The refractive indexes of the liquid deuterium (α-quartz) at 540 and 660 nm were 1.136 and 1.134 (1.546 and 1.542), respectively.

The shock-velocity histories of D_2 and the α-quartz were obtained using a two-channel VISAR [33]. The velocity sensitivities of different etalons produced by each fringe in vacuum are shown in Table I. The measured apparent velocity was then divided by the corresponding refractive index of each material at the probe wavelength to obtain the true velocity [32]. The VISAR system had a temporal resolution of $\sim$20 ps and a spatial resolution of $\sim$7 μm. The accuracy of the interference fringes was $\sim$5%, resulting in a velocity accuracy of less than 1%.

Figure 1(c) shows a typical VISAR image and shock-velocity profile of a single-shock and reflected-shock compression experiment. The probe beam passed through the transparent quartz and liquid deuterium in their initial state, reflected by the Al coating of the standard quartz. The main shock wave entered the standard quartz at $\sim$2.4 ns. Then, the VISAR fringe began to shift, corresponding to the shock velocity in the standard quartz, D_2, and the quartz window. Clear velocity jumps occurred at $\sim$5.5 ns, when the shock wave entered D_2, and at $\sim$8 ns, when the shock wave entered the quartz window.

B. Theoretical model

Up to now, the theoretical EOS of hydrogen and its isotopes could be divided into two categories. The first is the semiempirical models: modeling according to the phase structure of different thermodynamic regions, calculating the ionization based on chemical properties, and calibrating the models with experimental data; for thermodynamic regions with unclear chemical components, quantum molecular dynamics (QMD) and direct path-integral quantum Monte Carlo (QMC) methods are used to obtain theoretical data. The theoretical framework of multimodel integration is formed by integrating theoretical, experimental, and numerical simulation results, which is represented by a database or analytical-based model. The second one uses QMD and QMC simulations based on physical theories to obtain the theoretical data within a wide pressure area, which is represented by a database or fitting functions. Representatives of the first category include SESAME constructed by Kerley [36,37], SCvH by Saumon
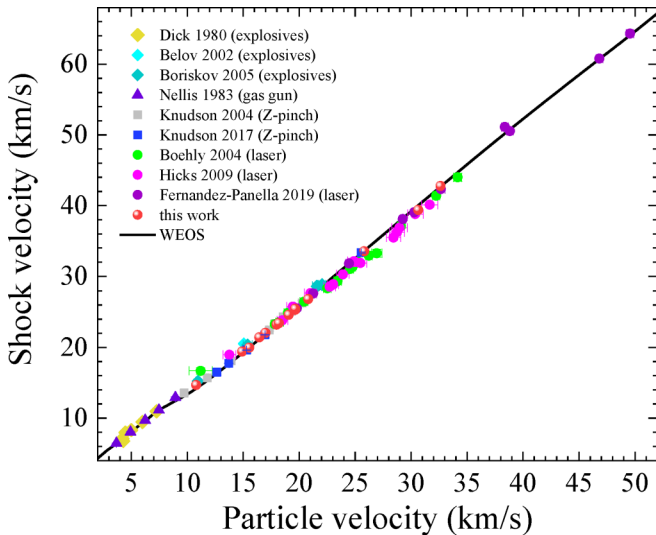
FIG. 2. Shock velocity vs particle velocity for the deuterium principal Hugoniot. Shown are the impedance-matching results for explosives from Ref. [49] (yellow diamonds), Ref. [50] (light cyan diamonds), and Ref. [18] (dark cyan diamonds); a gas gun from Ref. [16] (purple triangles); a magnetically driven flyer plate from Ref. [20] (gray squares) and Ref. [21] (blue squares); and laser-driven measurements from Ref. [51] (green circles), Ref. [22] (pink circles), and Ref. [23] (purple circles), and this work (red circles). The WEOS model ($\rho_0 = 0.170$ g/cm^3; black solid line) is also shown.

[38,39], REOS database by Nettelmann *et al.* [40] and wide-range EOS by Trunin *et al.* [41]. Representatives of the second category include the multiphase hydrogen EOS constructed by Caillabet *et al.* [42] which is based on the first-principles (FP) simulations, the restricted path-integral Monte Carlo simulation database published by Hu *et al.* [43], and the density functional theory (DFT) database developed by Wang and Zhang [44]. In fact, the first category is widely used in engineering applications due to the wide coverage of thermodynamic region and sufficient experimental verification. The second category of EOS with a wide pressure range is often used for validation and evaluation.

We constructed the WEOS of hydrogen's isotopes [45,46] using the semiempirical models which combine the improved chemical free-energy model [47], the FP numerical simulation results [45], and the multiparameter EOS model [48], which is applicable in the temperature range of 20–10^8 K and the density range of 10^{-7}–2000 g/cm^3 for hydrogen. In this work, the reshock states of WEOS are calculated based on the initial shock states of different experiments, which will be explained in the following sections.

III. RESULTS AND DISCUSSION

A. The principal Hugoniot

The principal Hugoniot data for cryogenic liquid deuterium are obtained via impedance matching and are listed in Table II. Our experimental data for the laser are compared with those of previous experiments on explosives [18,49,50], gas guns [16], Z machines [20,21], and lasers [22,23,51], as well as with different theoretical models (Figs. 2 and 3). Data from
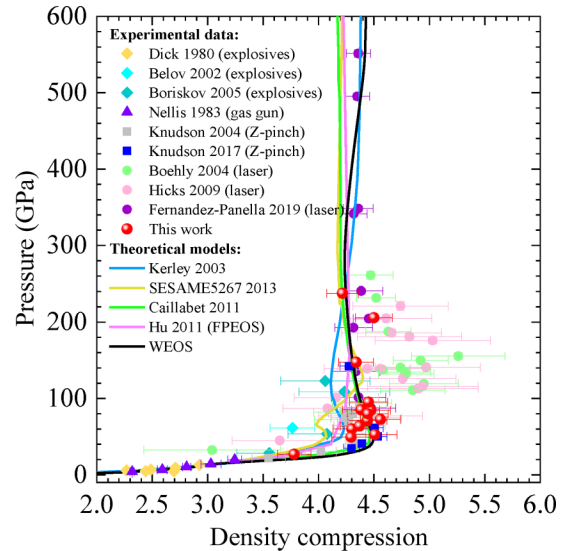

FIG. 3. Pressure vs compression plot of the principal Hugoniot of deuterium. Experimental data symbols are the same as in Fig. 2. All experimental data are plotted with error uncertainties. The data are compared to several EOS models: Kerley [37] (blue curve), Caillabet *et al.* [42] (green curve), FPEOS by Hu *et al.* [43] (pink curve), SESAME 5267 [39] (yellow curve), and WEOS ($\rho_0 = 0.170$ g/cm^3; black curve) [45,46].

Boehly *et al.* [51], Nellis *et al.* [16], and Knudson *et al.* [20] were reprocessed in later studies [21,22]. The relation of our shock velocity U_S and particle velocity u_p in D_2 is in good agreement with those of other experiments and theories. The slope of U_S relative to u_p decreases instantaneously when $u_p \sim 15$ km/s, illustrating the molecular dissociation in the MA transition and an increase in density as energy breaks bonds. The U_S-u_p relation can be expressed by piecewise fit [Eq. (B5)] of experimental data, which is used only in the data processing of reflected-shock results.

Figure 3 shows the pressure P vs compression η diagram of the principal Hugoniot of D_2. It shows our experimental data are in good agreement with the latest data of Knudson and Desjarlais [21] and Fernandez-Pañella *et al.* [23]. Especially for $50 < P < 100$ GPa, the centroid of our data is 4.29–4.56. The highest η of ∼4.56 is obtained near ∼70 GPa, consistent with the latest experimental data for Z pinches [21]. All these experiments are softer than the early data on Z pinches [20] in the range where the MA transition occurs. Establishing or selecting appropriate theoretical models is very necessary to accurately describe the EOS for hydrogen and its isotopes in a wide range. Here we do not discuss the technical details of this complex problem and only do some analysis from the direct comparison of experimental data and theories. All kinds of theoretical models are consistent at low pressure, in good agreement with Dick and Kerley [49], Nellis *et al.* [16], and our experiment at the lowest pressure of ∼27 GPa. For the onset of the MA transition (25–50 GPa), both WEOS [45,46] and Caillabet *et al.*'s model [42] are close to the latest Knudson and Desjarlais [21] data (blue squares in Fig. 3). For $50 < P < 100$ GPa, still, only the models of Caillabet *et al.* and WEOS agree with the most accurate

experiment. However, the density compression of two of our data points is ~4.3 (shots 14143 and 20083), which is ~4.6% smaller than that predicted by the two models. Both models show a maximum compression of ~4.5 near 50–70 GPa and then a decrease with increasing pressure. This is reasonable because the DFT molecular dynamics with the Perdew-Burke-Ernzerhof [52] exchange-correlation functional are performed in these two models. However, Fernandez-Pañella *et al.* show that chemical EOS models [37,39] underestimate the maximum compression by 4.5%–8%, and the first-principles EOS (FPEOS) model by Hu *et al.* [43] underestimated the maximum compression of deuterium by ~4.5%. At high pressure, the different calculation methods of molecular dissociation and atomic ionization of various theoretical models lead to the dispersion of theoretical models. When $100 < P < 240$ GPa, the models of Caillabet *et al.* and WEOS are still in good agreement with the experiment. However, with the increase of pressure to 560 GPa, the pressure and temperature exceed the applicable range of Caillabet *et al.*'s model [42], and the theory gradually deviates from the experimental data. When $P > 240$ GPa, interestingly, Kerley [37] predicted a significant increase in compressibility, which, together with the WEOS, was consistent with Fernandez-Pañella *et al.*'s experimental data. This shows that the calculation based on the chemical model at high pressure is reasonable. It should be noted that the initial density of WEOS in Fig. 3 is 0.170 g/cm^3. In fact, the tiny difference in the initial density will be reflected in the Hugoniot curve. We show the difference between the experiments and WEOS model at different initial densities in Fig. 8 in Appendix C. The evidence in Figs. 3 and 8 indicates that only WEOS meets the high-precision experimental data at 27–550 GPa (including data from Knudson and Desjarlais [21], Fernandez-Pañella *et al.* [23], and most of this work).

B. The reflected-shock Hugoniot

To better understand the high-pressure behavior of liquid deuterium, its reflected-shock state is determined using a shock-velocity measurement on both sides of the sample-window interface. The initial shock state here is not exactly the principal Hugoniot state of deuterium, but the state of deuterium when the shock wave reaches the sample-window interface, expressed as P_1^D, which can be determined by the observable shock velocity U_{S1}^D as well as Eq. (B5) and the Rankine-Hugoniot (RH) jump relations [53]. Then, the reshock state of the experiments can be obtained by the shock velocity of the quartz window U_{S1}^Q and applying the impedance-matching technique with the calibrated quartz (see Table III in Appendix B and Fig. 4). A reflected shock in one shot with an initial shock pressure P_1^D of ~32 GPa can reach ~116 GPa and a density of ~1.36 g/cm^3. In other shots, P_1^D of 43–240 GPa reaches 167–830 GPa after reflected shock in D_2, and the maximum density reaches ~1.49 g/cm^3, about 8.7 times the initial density. We extended the reflected shock data as low as 116 GPa and provide more data than Fernandez-Pañella *et al.* up to ~830 GPa with our new experiment.

In order to make a comparison with theoretical models we use the method introduced by Knudson and Desjarlais [21] to
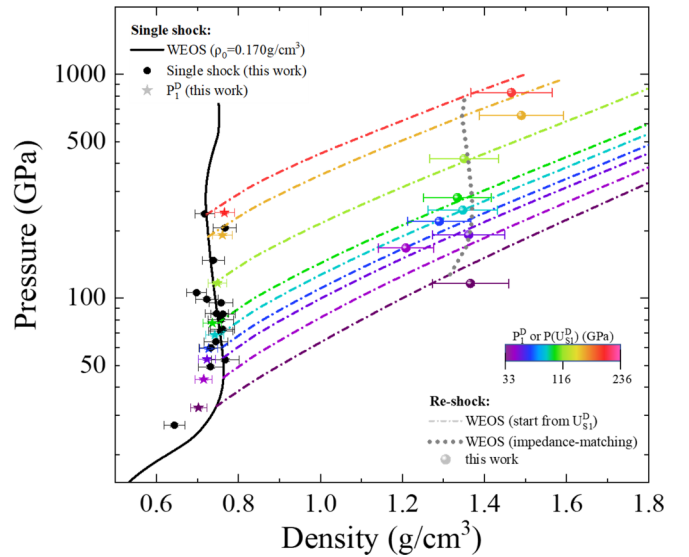

FIG. 4. Single-shock and reflected-shock pressure vs compressed densities of cryogenic liquid deuterium. Black circles correspond to single-shock data (Fig. 3). Stars correspond to (P_1^D, ρ_1^D) states from this work, the shocked state in D_2 prior to reflection by the quartz window (as the shock wave is not steady). Reshock states of deuterium from this work (solid circles) are shown. Dot-dashed lines are the WEOS model [45,46] calculated from $P(U_{S1}^D)$ of this work. The different colors of the P_1^D states and the reshock data represent different single-shock states. The dark gray dotted line is the WEOS model calculated by the impedance-matching technique with quartz.

determine the reshock Hugoniots of the WEOS model from different initial single shocks, shown as dot-dashed lines in different colors in Fig. 4. Here we define the initial state with an experimental observable, the shock velocity of deuterium's principal Hugoniot U_{S1}^D and the corresponding pressure $P(U_{S1}^D)$, according to the principal Hugoniot of WEOS because the measured U_{S1}^D can be used for different models to define other parameters (P_{1model}, ρ_{1model}, and $u_{p1model}$) and is thermodynamically consistent with the Hugoniot state. This is slightly different from that of Fernandez-Pañella *et al.*'s reshock Hugoniots from P_1^D. We believe doing so can lead to a more meaningful comparison with individual experiments. The difference between reshock Hugoniots calculated starting from P_1^D and U_{S1}^D is shown in Fig. 7(a) in Appendix B.

One method proposed by Fernandez-Pañella *et al.* [23] is to determine the model-predicted reflected-shock states by solving for the impedance-matching condition with a calibrated quartz Hugoniot for each model. We refer to this method to obtain the reshock state of WEOS. However, our approach is slightly different from Fernandez-Pañella *et al.*'s. Fernandez-Pañella *et al.* adjusted temperature T and internal energy E to force a model to match an inferred (not directly measured) density at a given Hugoniot pressure. In our opinion, we think this is not necessary because the matching result from $P(\rho, T)$ or $E(\rho, T)$ for the thermodynamically consistent model should be the same. We use the principal Hugoniot of WEOS as the initial state to calculate the reshock state through impedance matching with α-quartz, shown by the dark gray

dotted line in Fig. 4. This line, together with the reshock Hugoniots of WEOS calculated starting from different initial states U_{S1}^{D}, can confirm several intersections, which are the reshock states of WEOS (P_2^{D}, ρ_2^{D}).

We compare the reshock states of WEOS with experimental data of this work (Fig. 4), work of Fernandez-Pañella *et al.* [23] [Fig. 7(b)], and Knudson and Desjarlais [21] [Fig. 7(c)]. Obviously, the comparison between the WEOS model (intersections of reshock Hugoniots and reshock states) and experiments is more direct and intuitive. The pressure of intersections agrees with the experiments, but when the initial density in experiment is larger than the WEOS, the reshock density in experiment is basically also larger than the intersections produced by WEOS. So the comparison needs to be treated with caution because the deviation mainly comes from the differences between the initial shock density ρ_1 of the experiments and that of the WEOS. In order to obtain the quantitative comparison results, we have calculated the rms deviation of density and pressure between the intersections of WEOS and the three experimental works. The rms deviations of pressure (density) between experiments including this work, Fernandez-Pañella *et al.*'s work, and Knudson and Desjarlais's work with the WEOS model are 4.8% (6.4%), 1.5% (8.2%), and 2.9% (6.5%), respectively. Therefore, most of the reflected shock data, including ours, Fernandez-Pañella *et al.*'s, and Knudson and Desjarlais's are in accordance with our WEOS model in the dense, strongly coupled, partially degenerate fluid phase state up to 1 TPa. This result is different from Fernandez-Pañella *et al.*'s statement that experimental reshock compression of deuterium above 500 GPa is 5%–7% higher than the theoretical models of Kerley, Caillabet *et al.*, Hu *et al.*, and SESAME 5267.

IV. CONCLUSIONS

We have performed the principal Hugoniot and reflected-shock measurements of liquid deuterium in a wide pressure range. The maximum pressure of the principal Hugoniot and the reflected shock reach ∼240 and ∼830 GPa, respectively. For the principal Hugoniot, our experimental data broadly support models by Caillabet *et al.* and WEOS at 27–240 GPa, and only WEOS matches the latest high-precision experimental data up to ∼550 GPa. Our reshock density reaches ∼1.49 g/cm³, about 8.7 times the initial density. In this dense, strongly coupled, partially degenerate fluid phase state, our reshock data were compared with the latest experimental data using lasers and Z pinches under different single-shock states, showing that our data are consistent with the WEOS model. Thus, our independent principal and reflected experimental data well agree with the WEOS model within a wide pressure range (27–830 GPa), which provides an important benchmark for the development of the high-pressure response of hydrogen, directly related to ICF, planetary science, and metallization.

ACKNOWLEDGMENTS

APPENDIX A: DETAILS IN EXPERIMENTS AND DATA PROCESSING

1. Cryogenic experimental platform

A liquid deuterium cryogenic experimental platform was established to achieve low temperature from 12 to 300 K, reaching 12 K from room temperature within 80 min. The temperature measurement accuracy and control accuracy were ±0.01 and ±0.03 K, respectively. The liquefaction process was monitored using a charge-coupled device to ensure the deuterium was fully liquefied at ∼23 K. The experiment was conducted at ∼20.5 K. The initial density ρ_0 of the cryogenic liquid deuterium was 0.170 ± 0.001 g/cm³, calculated by the empirical formula [13,34,35] $\rho_0 = -0.005231T^3 + 0.3119T^2 - 8.225T + 252.9$, when $18.7 < T < 35$ K, where the units of ρ_0 are milligrams per cubic centimeter.

2. Velocity sensitivities of different etalons

The velocity sensitivities of different etalons produced by each fringe in vacuum at probe beam wavelengths of 540 and 660 nm are listed in Table I.

APPENDIX B: DEDUCING THE FIRST AND REFLECTED SHOCK STATES VIA THE IMPEDANCE-MATCHING TECHNIQUE

Impedance-matching measurements [14,26,27] were obtained as the shocks traversed the α-quartz-deuterium interface, enabling single-shock measurements at the first interface (pusher-sample) and reflected-shock measurements at the second interface (sample-window). With α-quartz (Al steps in two shots) as the reference standard, the particle velocity behind the shock wave in the D_2 sample was determined using the calibrated and extended quartz EOS [28–31]. For the two shots with the Al step as the standard reference, the particle velocity in D_2 was obtained using the calibrated linear relationship between aluminum's shock velocity and quartz's shock velocity [22]. However, clearly, quartz is the best choice. The uncertainties in the quartz EOS and release curves are propagated as systematic errors.

According to the impedance-matching technique and the following RH jump relations, the single-shock state of

TABLE I. Velocity per fringe (VPF) in vacuum of different etalons at 540 and 660 nm.

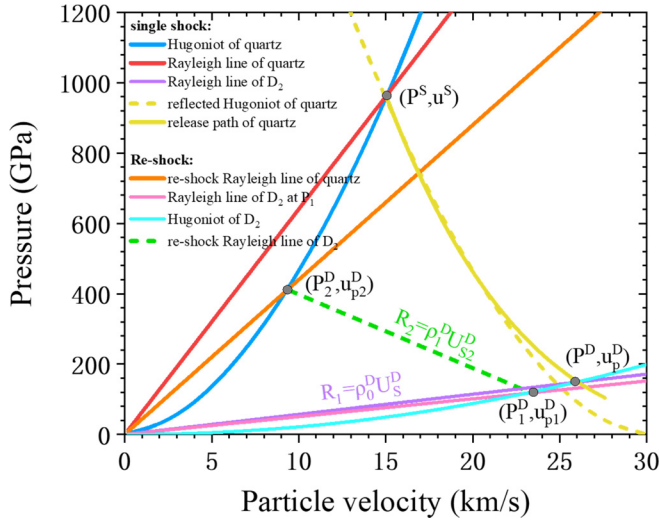| Etalon length (mm)	VPF_{540} (km/s)	VPF_{660} (km/s)
10.02	4.547	5.654
14.97	3.042	3.783
20.00	2.277	2.831
24.97	1.824	2.268
27.00	1.687	2.097

FIG. 5. P-u_p diagram illustrating the impedance-matching technique.

deuterium is

$$\rho_1 = \frac{\rho_0 U_{S_1}}{U_{S_1} - (u_{p_1} - u_{p_0})}, \tag{B1}$$

$$P_1 = P_0 + \rho_0 U_{S1}(u_{p1} - u_{p0}), \tag{B2}$$

$$E_1 = E_0 + \frac{1}{2}(P_1 + P_0)(V_0 - V_1), \tag{B3}$$

where ρ, U_S, and u_p represent density, shock velocity, and particle velocity, respectively. The subscripts 0 and 1 represent the initial and final values, respectively.

The shock state (P^S, u_p^S) of an α-quartz pusher was determined using the known Hugoniot of quartz standard [28,29] and the measured shock velocity of the quartz standard U_S^S (with an α-quartz standard as an example). The release path of α-quartz can then start from this point (Fig. 5). The Rayleigh line of deuterium is obtained from the shock velocity of deuterium, whose slope is $R_1 = \rho_0 U_S^D$. The intersection of the quartz's release path and the Rayleigh line of deuterium gives the single-shock state of deuterium (P^D, u_p^D). The remaining kinematic variables are determined using Eqs. (B1) and (B2). Using the Monte Carlo method and error transfer method, the 1σ uncertainties in u_p^D, P^D, and ρ^D are obtained (Table II). Since D_2 is a low-impedance material, the release path of quartz cannot be simply replaced by the reflected Hugoniot. The latest quartz release path by Desjarlais *et al.* [31] is used in this work. The key parameter of the release path, the effective Grüneisen constant Γ_{eff}, is expressed as

$$\Gamma_{\text{eff}} = \begin{cases} -1.4545 + 0.1102 U_s^Q \pm 0.036, & U_S^Q \leqslant 14.69 \text{ km/s}, \\ 0.579\{1 - \exp[-0.129(U_S^Q - 12.81)^{3/2}]\} \pm 0.036, & U_S^Q > 14.69 \text{ km/s}, \end{cases} \tag{B4}$$

where U_S^Q represents the shock velocity of quartz. As shown in Fig. 5 (shot 20079), initially, the release path drops below the reflected Hugoniot due to the higher sound velocity at high pressure. However, at lower pressures, the release path passes above the reflected Hugoniot. This is because the entropy of the release path is significantly higher than that of the reflected

TABLE II. Principal Hugoniot data determined using the impedance-matching technique with α-quartz or aluminum steps as the standard. The shock velocity of standard U_S^S and liquid deuterium U_S^D were used in impedance-matching analysis to determine the particle velocity u_p^D, pressure P^D, density ρ^D, and compression η^D of liquid deuterium at the standard-deuterium interface. The pulse width τ and wavelength λ of the driven laser are also listed.

Shot	τ (ns)	λ (nm)	U_S^S (km/s)	U_S^D (km/s)	u_p^D	P^D (GPa)	ρ^D (g/cm3)	η^D
14139[a]	3.00	351	19.33 ± 0.12	24.60 ± 0.15	19.06 ± 0.18	79.91 ± 1.22	0.757 ± 0.031	4.44 ± 0.18
14140[a]	3.00	351	16.73 ± 0.10	19.97 ± 0.12	15.54 ± 0.16	52.88 ± 0.83	0.768 ± 0.034	4.51 ± 0.20
14142	2.90	351	12.32 ± 0.08	14.69 ± 0.09	10.80 ± 0.14	27.04 ± 0.40	0.644 ± 0.026	3.78 ± 0.15
14143	2.97	351	15.50 ± 0.10	19.42 ± 0.12	14.90 ± 0.15	49.29 ± 0.63	0.732 ± 0.029	4.29 ± 0.17
15035	2.79	527	17.16 ± 0.11	22.05 ± 0.14	17.00 ± 0.16	63.89 ± 0.79	0.745 ± 0.029	4.37 ± 0.17
15037	2.86	527	18.09 ± 0.11	23.44 ± 0.15	18.19 ± 0.17	72.65 ± 0.88	0.761 ± 0.030	4.56 ± 0.18
16012	3.12	351	17.93 ± 0.11	23.21 ± 0.15	17.98 ± 0.17	71.12 ± 0.86	0.757 ± 0.030	4.44 ± 0.18
20079	2.93	351	24.17 ± 0.15	33.54 ± 0.21	25.81 ± 0.22	147.51 ± 1.67	0.739 ± 0.026	4.34 ± 0.16
20080	3.03	351	28.00 ± 0.18	39.39 ± 0.25	30.64 ± 0.25	205.63 ± 2.29	0.767 ± 0.028	4.50 ± 0.17
20082	3.01	351	29.64 ± 0.19	42.77 ± 0.27	32.63 ± 0.26	237.78 ± 2.63	0.718 ± 0.024	4.22 ± 0.14
20083	1.06	351	16.72 ± 0.10	21.42 ± 0.13	16.44 ± 0.16	60.01 ± 0.75	0.733 ± 0.029	4.30 ± 0.17
20085	1.06	351	19.26 ± 0.12	25.46 ± 0.16	19.65 ± 0.18	85.26 ± 1.01	0.747 ± 0.028	4.38 ± 0.17
20088	0.97	351	20.17 ± 0.13	26.84 ± 0.17	20.81 ± 0.19	95.16 ± 1.12	0.758 ± 0.029	4.45 ± 0.17
20092	2.13	351	19.25 ± 0.12	25.31 ± 0.16	19.65 ± 0.18	84.75 ± 1.01	0.762 ± 0.030	4.47 ± 0.18

[a]Aluminum was used as the standard material for impedance-matching in these shots.

TABLE III. Deuterium reshock data from impedance matching with α-quartz as the standard. U_{S1}^{Q} and U_{S1}^{D} are the measured shock velocity of the α-quartz window immediately after reshock and the deuterium shock velocity prior to reshock, respectively. We used a deuterium Hugoniot derived from the high-accuracy data shown in Fig. 2 to estimate particle velocity u_{p1}^{D} and the RH equations to estimate pressure P_{1}^{D} and density ρ_{1}^{D} along the Hugoniot. Then, using the Hugoniot of α-quartz, IM analysis, and RH equations, we derived the pressure P_{2}^{D}, density ρ_{2}^{D}, and particle velocity u_{p2}^{D} in the reshock state.

Shot	U_{S1}^{Q} (km/s)	U_{S1}^{D} (km/s)	u_{p1}^{D} (km/s)	P_{1}^{D} (GPa)	ρ_{1}^{D} (g/cm³)	u_{p2}^{D} (km/s)	P_{2}^{D} (GPa)	ρ_{2}^{D} (g/cm³)
14139	11.45 ± 0.07	18.28 ± 0.11	13.93 ± 0.09	43.38 ± 0.38	0.72 ± 0.02	5.52 ± 0.08	167.37 ± 3.46	1.21 ± 0.07
14140	9.41 ± 0.06	15.83 ± 0.10	11.99 ± 0.08	32.35 ± 0.29	0.70 ± 0.02	4.38 ± 0.08	116.16 ± 2.69	1.37 ± 0.09
15035	12.06 ± 0.08	20.22 ± 0.13	15.46 ± 0.10	53.26 ± 0.47	0.72 ± 0.02	5.99 ± 0.08	191.52 ± 3.82	1.36 ± 0.09
15037	12.74 ± 0.08	21.34 ± 0.13	16.34 ± 0.10	59.42 ± 0.53	0.73 ± 0.02	6.52 ± 0.08	220.26 ± 4.25	1.29 ± 0.08
16012	13.34 ± 0.08	22.87 ± 0.14	17.55 ± 0.11	68.39 ± 0.60	0.74 ± 0.02	6.99 ± 0.08	247.21 ± 4.65	1.35 ± 0.08
20079	16.60 ± 0.10	29.74 ± 0.19	22.97 ± 0.14	116.41 ± 1.03	0.75 ± 0.02	9.54 ± 0.09	419.67 ± 7.25	1.35 ± 0.08
20080	20.10 ± 0.13	38.03 ± 0.24	29.52 ± 0.18	191.27 ± 1.69	0.76 ± 0.02	12.27 ± 0.11	653.81 ± 10.77	1.49 ± 0.10
20082	22.31 ± 0.14	42.61 ± 0.27	33.13 ± 0.21	240.56 ± 2.13	0.77 ± 0.02	14.00 ± 0.12	827.79 ± 13.39	1.47 ± 0.10
20092	14.05 ± 0.09	24.30 ± 0.15	18.68 ± 0.12	77.34 ± 0.68	0.74 ± 0.02	7.55 ± 0.09	281.02 ± 5.16	1.33 ± 0.08

Hugoniot at a given volume, which increases the thermal pressure.

A series of (U_S^D, u_p^D) can be obtained via impedance-matching. Thus, the U_S^D-u_p^D relation can be expressed by piecewise fitting [Eq. (B5)]: The fitting data include the data from our experiments, low-pressure data from Dick and Kerley [49] and Nellis et al. [16], and the latest data from Knudson and Desjarlais [21] and Fernandez-Pañella et al. [23],

$$U_S^D = \begin{cases} -0.4593 + 1.3155 u_p^D, & u_p^D \geqslant 15.54 \text{ km/s,} \\ 2.6008 + 1.1177 u_p^D, & 3.676 \leqslant u_p^D < 15.54 \text{ km/s.} \end{cases}$$
(B5)

This U_S^D-u_p^D relation is also used in the data processing of reflected-shock results.

The determination of the reflected-shock pressure P_2^D and density ρ_2^D of deuterium is shown in Fig. 5. After the single shock at the quartz-sample interface, the initial shock velocity of deuterium U_{S1}^D at the sample-window interface is also measured. U_{S1}^Q in the rear quartz window provides (P_2^D, u_{p2}^D) of the reflected-shock deuterium. Then, the slope of the Rayleigh line of the reflected shock in deuterium is determined using the RH jump relation, $R_2 = (P_2^D - P_1^D)/(u_{p2}^D - u_{p1}^D) = \rho_1 U_{S2}^D$. The density of reflected-shock deuterium is then obtained using Eq. (B1), $\rho_2^D = \rho_1^D [U_{S2}^D/(U_{S2}^D - (u_{p2}^D - u_{p1}^D))]$. Using the Monte Carlo method, the 1σ uncertainties of the reshock state are listed in Table III and shown in Fig. 4.

Figure 6 depicts the observable U_{S1}^D measured before reflection by the α-quartz window and U_{S1}^Q measured immediately after reshock, as well as the experimental data and EOS models from previous work. Our data cover the shock velocity of D_2 from 15.83 to 42.61 km/s. These data generally manifest as a linear law with good consistency, but the slope below 22 km/s is larger. This area is exactly where the MA transition occurs, and the compressibility of the principal Hugoniot changes suddenly. The top illustration in Fig. 6 shows the residuals of the velocity data and EOS models when normalized to the WEOS model. Compared with other theoretical

models, it seems that WEOS is closer to the centroids of the experimental data on average.

Figures 7(a), 7(b), and 7(c) show the comparisons of the reshock states of the WEOS model and that of Caillabet et al. with experiments from this work and work of Fernandez-
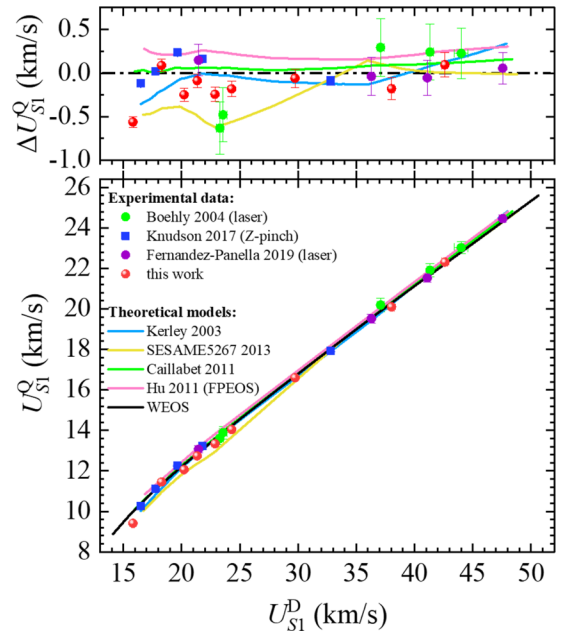

FIG. 6. Experimental observables for the reflected-shock experiments, U_{S1}^Q vs U_{S1}^D, from this study are red solid circles. Previous z-pinch data from Knudson and Desjarlais [21] (gray squares) and laser-driven data from Boehly et al. [51] (green circles) and Fernandez-Pañella et al. [23] (purple circles) are also shown. All experimental data are plotted with error uncertainties. The colored solid lines correspond to the predictions of EOS models, which are the same as in Fig. 3. The velocity residuals of the different data sets and EOS models with respect to the WEOS model are shown in the top illustration. The initial density of the experiments in this work and the WEOS model is 0.170 g/cm³, while other theoretical models quoted correspond to an initial density of 0.173 g/cm³ [23].
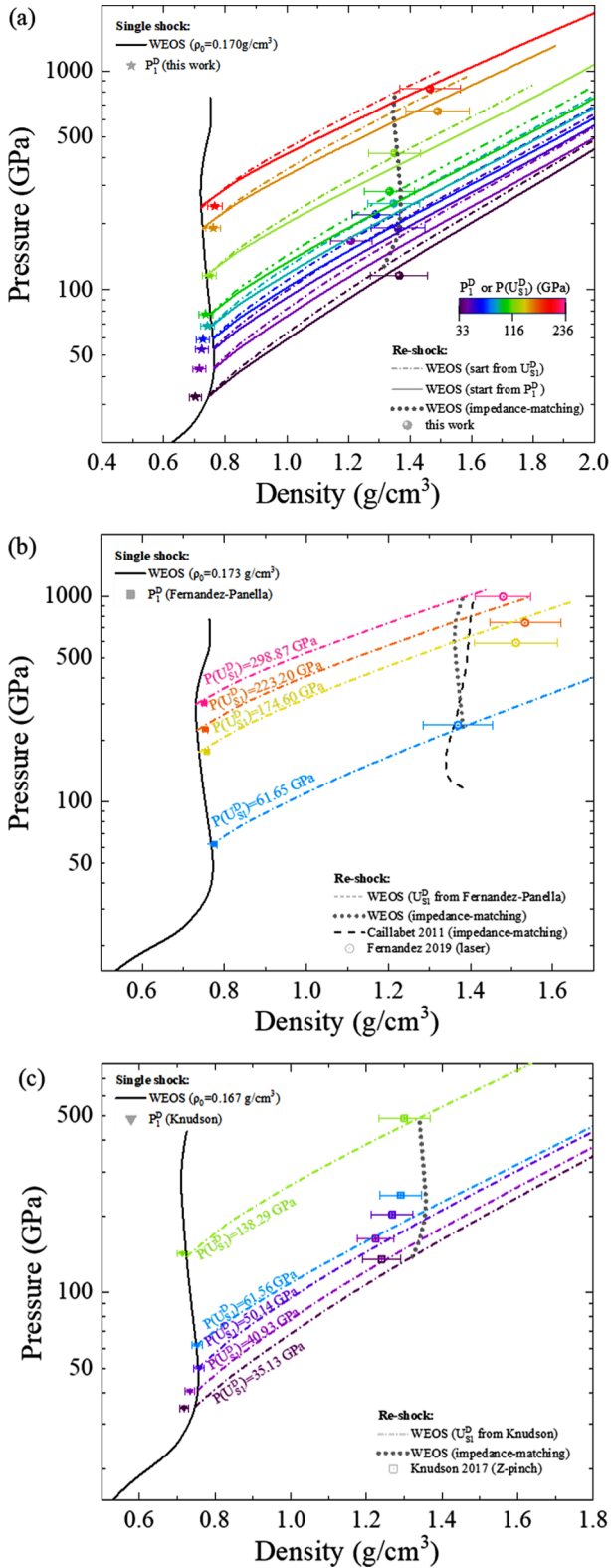
FIG. 8. P-ρ diagram illustrating the initial density effects of liquid deuterium.

FIG. 7. P_1^D and reflected-shock pressure vs compressed densities of cryogenic liquid deuterium of (a) this work, (b) Fernandez-Pañella *et al.* [23], and (c) Knudson and Desjarlais [21]. The reshock states starting from various initial states U_{S1}^D of the three experiments are calculated with the WEOS model. The dark gray dotted line (black long-dashed lines) are the WEOS model (Caillabet *et al.*'s [42] model) calculated with the impedance-matching technique proposed by Fernandez-Pañella *et al.*
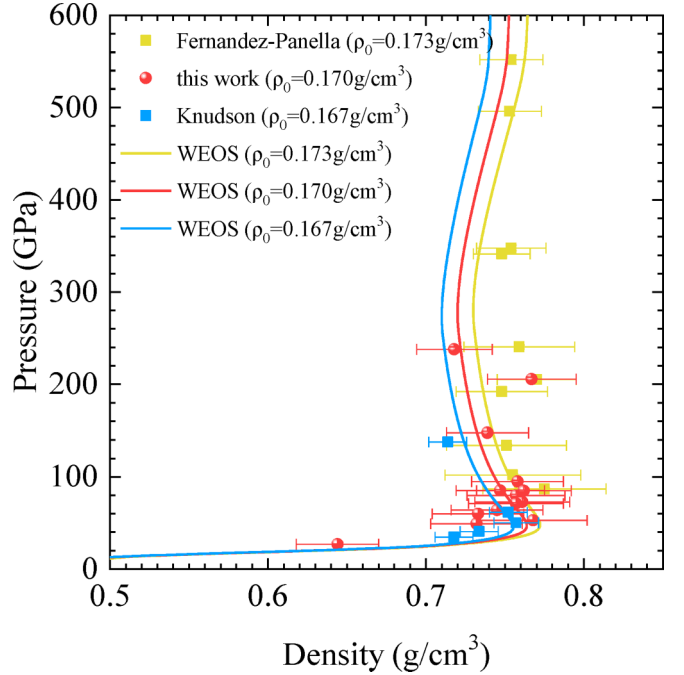
Pañella *et al.* and Knudson and Desjarlais considering the differences of the initial densities among these works. These three plots are used as a supplement to Fig. 4 in the main text in order to make the comparison between the experiments and the WEOS model clearer. See the main text for details. We determine the corresponding pressure as $P(U_{S1}^D)$ from the initial state with U_{S1}^D according to the principal Hugoniot of WEOS rather than P_1^D. The differences in the reshock lines starting from $P(U_{S1}^D)$ (colored dot-dashed lines) and P_1^D (colored solid lines) are shown in Fig. 7(a). Obviously, the reshock pressure (intersections of solid lines or dot-dashed lines with the dark gray dotted line) agrees well with experiment from U_{S1}^D.

APPENDIX C: INITIAL DENSITY EFFECTS ON THE PRINCIPLE HUGONIOT OF LIQUID DEUTERIUM

The deuterium Hugoniot experiments carried out at the various facilities were performed with different initial densities. The tiny difference in initial density will affect the Hugoniot results. The initial densities of this work, Fernandez-Pañella *et al.*, and Knudson and Desjarlais are determined by the definite temperature of cryogenic liquid deuterium through the calculations of the empirical formula [13,34,35]. Since the accuracy of temperature control can reach ± 0.03 K, the uncertainty of initial densities is as small as 0.001 g/cm^3. The initial densities of cryogenic liquid deuterium of this work, Fernandez-Pañella *et al.*, and Knudson and Desjarlais are 0.170, 0.173, and 0.167 g/cm^3, respectively. The corresponding theoretical Hugoniot curves of the three initial densities calculated by WEOS are shown in Fig. 8. An error of ~1.8% in initial density will lead to an error of ~1.4% in Hugoniot density at ~240 GPa.

[1] J. M. McMahon, M. A. Morales, C. Pierleoni, and D. M. Ceperley, The properties of hydrogen and helium under extreme conditions, Rev. Mod. Phys. **84**, 1607 (2012).

[2] D. J. Stevenson, Interiors of the giant planets, Annu. Rev. Earth Planet Sci. **10**, 257 (1982).

[3] D. Saumon, G. Chabrier, and H. M. V. Horn, An equation of state for low-mass stars and giant planets, Astrophys. J. Suppl. **99**, 713 (1995).

[4] W. B. Hubbard and B. Militzer, A preliminary jupiter model, Astrophys. J. **820**, 80 (2016).

[5] L. B. Da Silva, P. Celliers, G. W. Collins, K. S. Budil, N. C. Holmes, T. W. Barbee, Jr., B. A. Hammel, J. D. Kilkenny, R. J. Wallace, M. Ross, R. Cauble, A. Ng, and G. Chiu, Absolute Equation of State Measurements on Shocked Liquid Deuterium up to 200 GPa (2 mbar), Phys. Rev. Lett. **78**, 483 (1997).

[6] J. D. Lindl, P. Amendt, R. L. Berger, S. G. Glendinning, S. H. Glenzer, S. W. Haan, R. L. Kauffman, O. L. Landen, and L. J. Suter, The physics basis for ignition using indirect-drive targets on the national ignition facility, Phys. Plasmas **11**, 339 (2004).

[7] O. A. Hurricane, D. A. Callahan, D. T. Casey, P. M. Celliers, C. Cerjan, E. L. Dewald, T. R. Dittrich, T. Döppner, D. E. Hinkel, L. F. Berzak Hopkins, J. L. Kline, S. Le Pape, T. Ma, A. G. MacPhee, J. L. Milovich, A. Pak, H.-S. Park, P. K. Patel, B. A. Remington, J. D. Salmonson, P. T. Springer, and R. Tommasini, Fuel gain exceeding unity in an inertially confined fusion implosion, Nature (London) **506**, 343 (2014).

[8] S. L. Pape, L. F. B. Hopkins, L. Divol, and A. Pak, Fusion Energy Output Greater Than the Kinetic Energy of an Imploding Shell at the National Ignition Facility, Phys. Rev. Lett. **120**, 245003 (2018).

[9] D. E. Fratanduono, M. Millot, A. Fernandez Pañella, P. A. Sterne, G. W. Collins, D. G. Hicks, J. H. Eggert, T. R. Boehly, and P. M. Celliers, Measurement of the sound speed in dense fluid deuterium along the cryogenic liquid hugoniot, Phys. Plasmas **26**, 012710 (2019).

[10] E. Wigner and H. B. Huntington, On the possibility of a metallic modification of hydrogen, J. Chem. Phys. **3**, 764 (1935).

[11] P. M. Celliers, G. W. Collins, L. B. Da Silva, D. M. Gold, R. Cauble, R. J. Wallace, M. E. Foord, and B. A. Hammel, Shock-Induced Transformation of Liquid Deuterium into a Metallic Fluid, Phys. Rev. Lett. **84**, 5564 (2000).

[12] T. Sano *et al.*, Laser-shock compression and hugoniot measurements of liquid hydrogen to 55 GPa, Phys. Rev. B **83**, 054117 (2011).

[13] Z. He, G. Jia, F. Zhang, K. Luo, X. Huang, H. Shu, Z. Fang, J. Ye, Z. Xie, and M. Xia, Thermodynamic and electrical properties of laser-shocked liquid deuterium, Eur. Phys. J. D **72**, 3 (2018).

[14] Y. Zeldovich and Y. Raizer, *Physics of Shock Waves and High-Temperature Hydrodynamic Phenomena* (Academic, New York, 1966).

[15] W. J. Nellis, Shock Compression of Deuterium near 100 GPa Pressures, Phys. Rev. Lett. **89**, 165502 (2002).

[16] W. J. Nellis, A. C. Mitchell, M. V. Thiel, G. J. Devine, R. J. Trainor, and N. Brown, Equation-of-state data for molecular hydrogen and deuterium at shock pressures in the range 2–76 GPa (20–760 kbar), J. Chem. Phys. **79**, 1480 (1983).

[17] G. V. Boriskov, A. I. Bykov, R. I. Il'kaev, V. D. Selemir, G. V. Simakov, R. F. Trunin, V. D. Urlin, V. E. Fortov, and A. N. Shuikin, Shock-wave compression of solid deuterium at a pressure of 120 GPa, Dokl. Phys. **48**, 553 (2003).

[18] G. V. Boriskov, A. I. Bykov, R. I. Il'Kaev, V. D. Selemir, G. V. Simakov, R. F. Trunin, V. D. Urlin, A. N. Shuikin, and W. J. Nellis, Shock compression of liquid deuterium up to 109 GPa, Phys. Rev. B **71**, 092104 (2005).

[19] S. K. Grishechkin, V. K. Gruzdev, S. K. Gryaznov, M. V. Zhernokletov, R. I. Il'kaev, I. L. Iosilevskii, G. N. Kashintseva, S. I. Kirshanov, S. F. Manachkin, and V. B. Mintsev, Experimental measurements of the compressibility, temperature, and light absorption in dense shock-compressed gaseous deuterium, JETP Lett. **80**, 398 (2004).

[20] M. D. Knudson, D. L. Hanson, J. E. Bailey, C. A. Hall, J. R. Asay, and C. Deeney, Principal Hugoniot, reverberating wave, and mechanical reshock measurements of liquid deuterium to 400 GPa using plate impact techniques, Phys. Rev. B **69**, 144209 (2004).

[21] M. D. Knudson and M. P. Desjarlais, High-Precision Shock Wave Measurements of Deuterium: Evaluation of Exchange-Correlation Functionals at the Molecular-To-Atomic Transition, Phys. Rev. Lett. **118**, 035501 (2017).

[22] D. G. Hicks, T. R. Boehly, P. M. Celliers, J. H. Eggert, S. J. Moon, D. D. Meyerhofer, and G. W. Collins, Laser-driven single shock compression of fluid deuterium from 45 to 220 GPa, Phys. Rev. B **79**, 014112 (2009).

[23] A. Fernandez-Pañella, M. Millot, D. E. Fratanduono, M. P. Desjarlais, S. Hamel, M. C. Marshall, D. J. Erskine, P. A. Sterne, S. Haan, T. R. Boehly, G. W. Collins, J. H. Eggert, and P. M. Celliers, Shock Compression of Liquid Deuterium up to 1 TPa, Phys. Rev. Lett. **122**, 255702 (2019).

[24] X. Deng, X. Liang, Z. Chen, W. Yu, and R. Ma, Uniform illumination of large targets using a lens array, Appl. Opt. **25**, 377 (1986).

[25] S. Fu, Y. Gu, J. Wu, and S. Wang, Laser-driven shock stability in Al and shock compressibilities of Fe up to 0.8 TPa and SiO$_2$ up to 0.4 TPa, Phys. Plasmas **2**, 3461 (1995).

[26] P. M. Celliers, G. W. Collins, D. G. Hicks, and J. H. Eggert, Systematic uncertainties in shock-wave impedance-match analysis and the high-pressure equation of state of Al, J. Appl. Phys. **98**, 113529 (2005).

[27] S. Fu, X. Huang, M. Ma, H. Shu, J. Wu, J. Ye, J. He, Y. Gu, P. Luo, and T. Rong, Analysis of measurement error in the experiment of laser equation of state with impedance-match way and the Hugoniot data of Cu up to 2.24TPa with high precision, J. Appl. Phys. **101**, 043517 (2007).

[28] M. D. Knudson and M. P. Desjarlais, Shock Compression of Quartz to 1.6 TPa: Redefining a Pressure Standard, Phys. Rev. Lett. **103**, 225501 (2009).

[29] M. D. Knudson and M. P. Desjarlais, Adiabatic release measurements in α-quartz between 300 and 1200 GPa: Characterization of α-quartz as a shock standard in the multimegabar regime, Phys. Rev. B **88**, 184107 (2013).

[30] S. Brygoo, M. Millot, P. Loubeyre, A. E. Lazicki, S. Hamel, T. Qi, P. M. Celliers, F. Coppari, J. H. Eggert, and D. E. Fratanduono, Analysis of laser shock experiments on precompressed samples using a quartz reference and application to warm dense hydrogen and helium, J. Appl. Phys. **118**, 195901 (2015).

[31] M. P. Desjarlais, M. D. Knudson, and K. R. Cochrane, Extension of the Hugoniot and analytical release model of a-quartz to 0.2-3 TPa, J. Appl. Phys. **122**, 035903 (2017).

[32] P. M. Celliers, D. K. Bradley, G. W. Collins, D. G. Hicks, T. R. Boehly, and W. J. Armstrong, Line-imaging velocimeter for shock diagnostics at the OMEGA laser facility, Rev. Sci. Instrum. **75**, 4916 (2004).

[33] H. Shu, S. Fu, X. Huang, J. Wu, Z. Xie, F. Zhang, J. Ye, G. Jia, and H. Zhou, Measuring preheat in laser-drive aluminum using velocity interferometer system for any reflector: Experiment, Phys. Plasmas **21**, 082708 (2014).

[34] R. D. Goodwin, D. E. Diller, H. M. Roder, and L. A. Weber, The densities of saturated liquid hydrogen, Cryogenics **2**, 81 (1961).

[35] P. C. Souers, *Hydrogen Properties for Fusion Energy* (University of California Press, Berkeley, 1986).

[36] G. I. Kerley, Equation of state and phase diagram of dense hydrogen, Phys. Earth Planet. Inter. **6**, 78 (1972).

[37] G. I. Kerley, Sandia National Laboratories, Technical Report No. SAND2003-3613, 2003 (unpublished).

[38] D. Saumon, A new tabular EOS for hydrogen isotopes, AIP Conf. Proc. **955**, 101 (2007).

[39] D. Saumon, Los Alamos National Laboratory, Technical Report No. LA-UR-13-20032, 2013 (unpublished).

[40] N. Nettelmann, A. Becker, B. Holst, and R. Redmer, Jupiter models with improved ab initio hydrogen equation of state (h-reos.2), Astrophys. J. **750**, 52 (2012).

[41] R. F. Trunin, V. D. Urlin, and A. B. Medvedev, Dynamic compression of hydrogen isotopes at megabar pressures, Phys. Usp. **53**, 577 (2010).

[42] L. Caillabet, S. Mazevet, and P. Loubeyre, Multiphase equation of state of hydrogen from *ab initio* calculations in the range 0.2 to 5 g/cc up to 10 eV, Phys. Rev. B **83**, 094101 (2011).

[43] S. X. Hu, B. Militzer, V. N. Goncharov, and S. Skupsky, First-principles equation-of-state table of deuterium for inertial confinement fusion applications, Phys. Rev. B **84**, 224109 (2011).

[44] C. Wang and P. Zhang, Wide range equation of state for fluid hydrogen from density functional theory, Phys. Plasmas **20**, 092703 (2013).

[45] H. Liu, G. Zhang, Q. Zhang, H. Song, Q. Li, Y. Zhao, B. Sun, and H. Song, Progress on equation of state of hydrogen and deuterium, Chin. J. High Pressure Phys. **32**, 050101 (2018).

[46] H. Liu, Q. Li, Q. Zhang, G. Zhang, H. Song, Y. Zhao, B. Sun, and H. Song, Progress on wide-range equation of state for hydrogen and deuterium, High Power Laser Part. Beams **33**, 012003 (2021).

[47] Q. Li, H. Liu, G. Zhang, and Q. Zhang, Application of simulated annealing method in chemical free energy model, Chin. J. Comput. Phys. **10**, 19596 (2018).

[48] I. A. Richardson, J. W. Leachman, and E. W. Lemmon, Fundamental equation of state for deuterium, J. Phys. Chem. Ref. Data **43**, 013103 (2014).

[49] R. D. Dick and G. I. Kerley, Shock compression data for liquids. II. Condensed hydrogen and deuterium, J. Chem. Phys. **73**, 5264 (1980).

[50] S. I. Belov, G. V. Boriskov, A. I. Bykov, R. I. Il'kaev, N. B. Luk'yanov, A. Ya. Matveev, O. L. Mikhailova, V. D. Selemir, G. V. Simakov, R. F. Trunin, I. P. Trusov, V. D. Urlin, V. E. Fortov, and A. N. Shuikin, Shock compression of solid deuterium, JETP Lett. **76**, 433 (2002).

[51] T. R. Boehly, D. G. Hicks, P. M. Celliers, T. J. B. Collins, R. Earley, J. H. Eggert, D. Jacobs-Perkins, S. J. Moon, E. Vianello, D. D. Meyerhofer, and G. W. Collins, Properties of fluid deuterium under double-shock compression to several mbar, Phys. Plasmas **11**, L49 (2004).

[52] J. P. Perdew, K. Burke, and M. Ernzerhof, Generalized Gradient Approximation Made Simple, Phys. Rev. Lett. **77**, 3865 (1996).

[53] G. Duvall and R. Graham, Phase transitions under shock-wave loading, Rev. Mod. Phys. **49**, 523 (1977).